JOURNAL OF CATALYSIS **173,** 219–228 (1998)
ARTICLE NO. CA971909

The Protonation of MoO_3 during the Partial Oxidation of Alcohols

Richard L. Smith and Gregory S. Rohrer[1]

Department of Materials Science and Engineering, Carnegie Mellon University, Pittsburgh, Pennsylvania 15213-3890

Received July 10, 1997; revised September 22, 1997; accepted September 23, 1997

Atomic force microscopy and X-ray diffraction have been used to characterize the structural evolution of the MoO_3(010) surface during gas phase reactions with nitrogen-alcohol (methanol, ethanol, and 2-propanol) mixtures between 200 and 400°C. Our results demonstrate that MoO_3 intercalates H during these reactions ($T \geq 300$°C) and that protonation leads to the precipitation of a well known hydrogen molybdenum bronze, H_xMoO_3, where $0.23 \leq x \leq 0.4$. The acicular precipitates of H_xMoO_3 form topotactically and are aligned along the ⟨203⟩ directions of the MoO_3(010) surface plane. Identical H_xMoO_3 precipitates form when MoO_3 (010) surfaces are reacted with atomic H produced by "spill over" from supported Pt particles. The mechanism by which MoO_3 oxidizes alcohols, and the potential role of the protonated phase in this reaction, is reexamined in the context of these new observations.

INTRODUCTION

The results of O^{18} isotopic labeling experiments (1) and temperature programmed desorption (TPD) spectroscopy (2–4) studies support the conclusion that the selective oxidation of methanol and ethanol by MoO_3 can be described by a redox mechanism of the Mars-van Krevelen type (5). In other words, the catalyst acts as a renewable oxygen source that is able to create and annihilate stoichiometry compensating defects as it is reduced and reoxidized during the reaction. Because the mechanisms by which MoO_3 accommodates non-stoichiometry are believed to influence its reactivity (6), a number of investigators have previously studied its bulk structural evolution during reduction reactions. X-ray diffraction (XRD) studies have demonstrated that when MoO_3 is reduced by methanol at 200–215°C, the oxide is converted to a H-bronze phase, H_xMoO_3 (7, 8). Numerous transmission electron microscopy (TEM) studies (9–23) have shown that a domain microstructure develops during the early stages of all reduction treatments, but this observation has not always been interpreted in the same way. In the most recent study, the notion that a H-bronze forms during reduction by methanol was rejected (21), despite compelling evidence from earlier diffraction studies (7, 8, 15). We have more recently reported the results of an atomic force microscopy (AFM) study of the evolution of the MoO_3(010) surface during reduction in 10% H_2–N_2 at 400°C (24). The utility of this surface sensitive perspective was demonstrated by the observation that small pits and new surface sites form on the basal plane during reduction in hydrous environments. In this paper, we describe the results of AFM and X-ray diffraction (XRD) experiments designed to determine how the MoO_3(010) surface is altered by reactions with alcohol-nitrogen mixtures between 200 and 400°C. Our results lead to the conclusion that a H-bronze phase is formed during alcohol oxidation and, therefore, provide evidence for a second and fundamentally different mechanism by which the oxide is reduced during reactions with alcohols; in addition to losing oxygen, MoO_3 intercalates H removed from the alcohol.

METHODS

(a) MoO_3 Sample Preparation

Single crystals of α-MoO_3 were grown by a previously described chemical vapor transport method (24, 25). To facilitate cleavage and sample manipulation, each single crystal sample was mounted on a steel disc (d = 1 cm, t = 0.072 cm) by spot welding a thin strip of Ta foil across its (010) facet. Fresh (010) surfaces could then be prepared by cleavage with adhesive tape immediately before the reaction. To verify that our mounting materials and cleavage procedure did not influence the surface-structural evolution during the reactions, we also examined a limited number of unmounted crystals that were either not cleaved or cleaved with a razor blade and then reacted in a silica boat. These procedures did not influence the observed microstructural changes.

To study the evolution of the MoO_3(010) surface during reactions with atomic H, produced by H "spill over" (26–30), Pt-supporting MoO_3 samples were prepared. Pt

[1] Author to whom correspondence should be addressed. Fax: 412-268-7596. E-mail: gr20@andrew.cmu.edu. www: http://neon.mems.cmu.edu/rohrer.html.

0021-9517/98 $25.00

particles were deposited on these samples by dipping cleaved, mounted single crystals in a dilute (0.08 w/o) suspension of Pt black in methanol. The solvent was then evaporated by heating the sample overnight in air at 160°C.

(b) Surface Reactions

The single crystal samples were reacted under a continuous gas flow in a quartz reaction tube (i.d. = 19 mm, length = 1 m). The hot-zone of the reactor was heated by a nichrome tube furnace and had a length of 0.3 m. The temperature of the hot-zone was monitored with an alumina-clad, type-K thermocouple that was fed into the reactor by way of a Pyrex, compression-type gasket fitting. A magnetic transfer rod was used to move the sample between the hot and cold-zones of the reactor. The transfer rod consisted of a quartz tube (length = 30 cm, i.d. = 0.8 cm) within which a permanent magnet was sealed. The mounted sample was held in place on the quartz rod by clips fashioned from chromel wire.

Prior to reaction, the single crystal sample was cleaved in the ambient. It was then placed on the magnetic transfer rod and the assembly was immediately loaded into the cold-zone of the reactor under a flow of the reactant gas mixture of interest. With the hot-zone of the reaction tube at temperature and the sample still in the cold-zone, the reactor was purged three times by alternately evacuating (with an oil-less pump) and backfilling with the reactant gas mixture of interest. The sample was then transferred to the hot-zone of the reactor, positioned adjacent to the thermocouple, and allowed to react for a pre-determined period of time under the desired gas flow. The reaction was concluded by transferring the sample back to the cold-zone of the reactor and allowing it to cool to room temperature under a flow of gas (either the reaction mixture of dry N_2). In timing the reactions, the reaction was taken to start when the sample temperature was within 5% of the desired temperature and end when the sample was transferred back to the cold-zone of the reactor.

By using the magnetic transfer rod for sample manipulation within the reactor, it was possible to heat, react, and cool the sample without exposing it or the reaction system to the ambient after the system was purged. Due to the low thermal mass of the sample and transfer rod, it typically took less than 30 s to heat the sample to within 5% of the desired reaction temperature and the actual temperature never exceeded the desired by more than 5%. Control experiments were also conducted without the thermocouple and transfer rod. In these experiments, the reactor temperature was monitored *ex situ* and the sample was heated and cooled by sliding the reaction tube into or out of the furnace. While it was still possible to conduct the reaction without exposing the system to the ambient after the purge, it took up to 2 min to heat these samples to the desired reaction temperature. These control experiments demonstrated that the presence of Al_2O_3, chromel, and alumel in the reactor did not influence the evolution of the MoO_3(010) surface.

All of the alcohol reactions were performed at a total pressure of 1 atm in a 200 cc/min flow of N_2–ROH (where R is CH_3=Me, C_2H_5=Et, C_3H_7=2-Pr). The temperature range between 200 and 400°C was investigated. Because residual water vapor has been shown to influence the evolution of the MoO_3(010) surface during reduction (24), the N_2 (Prepurified, Matheson) carrier gas was dried prior to saturating it with alcohol in a bubbler. The N_2 was first passed through a tube of Cu metal turnings at 400°C and then through a column of $CaSO_4$ (Drierite). The temperature of the alcohol bubbler was maintained at 0°C for reactions with MeOH (99.9+%, Aldrich) and EtOH (Absolute, McCormick) and at 25°C for 2-PrOH (Certified, Fisher). Additional experiments were also conducted with 200 cc/min flows of N_2, 10% H_2–N_2 (forming gas), and CO.

For the hydrogen spill over experiments, the Pt-supporting samples were reacted in a 200 cc/min flow of dry forming gas at temperatures between 25 and 200°C. Experiments were also conducted with excess Pt. These samples were prepared by sprinkling a ~1 mm thick layer of Pt black on a cleaved, mounted single crystal which was held in an alumina crucible. To avoid contaminating the reaction tube with Pt, the Pt-excess samples were reacted in a flow of dry forming gas in a Pyrex 3-neck flask which was heated with a spherical, resistive heating mantel. At the conclusion of the reaction, the surface was blasted with N_2 to remove excess Pt. Finally, experiments were also conducted in dry CO and N_2 to verify that the observed microstructural changes were the result of H intercalation and not oxygen loss.

(c) AFM Analysis

Once a reacted sample had cooled to room temperature, it was removed from the reactor and immediately imaged in the ambient atmosphere with a Digital Instruments Nanoscope Multimode SPM or a Park Scientific Instruments Autoprobe CP. The microscopes were operated in contact mode (constant force) using pyramidal Si_3N_4 or conical Si cantilevered-tips and forces between 0.1 and 8 nN. Each sample was, typically, imaged for several hours and changes in surface topography over the analysis period were not observed.

Although the majority of our AFM observations were recorded in air, controlled environment experiments demonstrated that the ambient observations were not influenced by room temperature air, as long as the exposure was limited to a few days. By conducting the experiments in a short reaction tube (l = 30 cm) with stopcocks at both ends, it was possible to seal the reactor off after the treatment and transfer the sample, without exposure to air, to an AFM operated in a glove box filled with continuously purified Ar. The surface structural evolution observed in dry Ar was indistinguishable from that observed in ambient air.

(d) X-Ray Diffraction

X-ray diffraction was used to identify any new phases that may have formed during the reactions. To establish phase identity on single crystal surfaces, X-ray samples were prepared in the following way. First, 5–10 single crystals were reacted simultaneously in a silica boat. To selectively probe material from the near surface region, the reacted (010) surface layers were then cleaved from the crystals with adhesive tape (the layers were each less than 20 μm thick), pulverized, and immediately subjected to X-ray analysis. Due to the small quantity of material available for X-ray analysis, the samples were mounted by sprinkling the powder on a glass slide which was coated with a layer of double-stick tape. At least one of the reacted crystals from each batch was characterized with AFM to ensure that the MoO_3(010) surface structure could be directly correlated with the X-ray data.

In some cases, parallel experiments were conducted with powdered MoO_3 samples. These samples were reacted in a silica boat in the same reactor that was utilized for the single crystal studies. Standard mounting procedures were employed and powdered Si was used as an internal standard. All X-ray data were recorded in the ambient on a Rigaku Θ-2Θ powder diffractometer using a step size of 0.05° in 2Θ and Cu K_α radiation generated by a source operated at 35 kV and 25 mA. To obtain lattice parameters, the diffraction data were refined using a least-squares method. Typically, the first 10–15 peaks were included in this refinement.

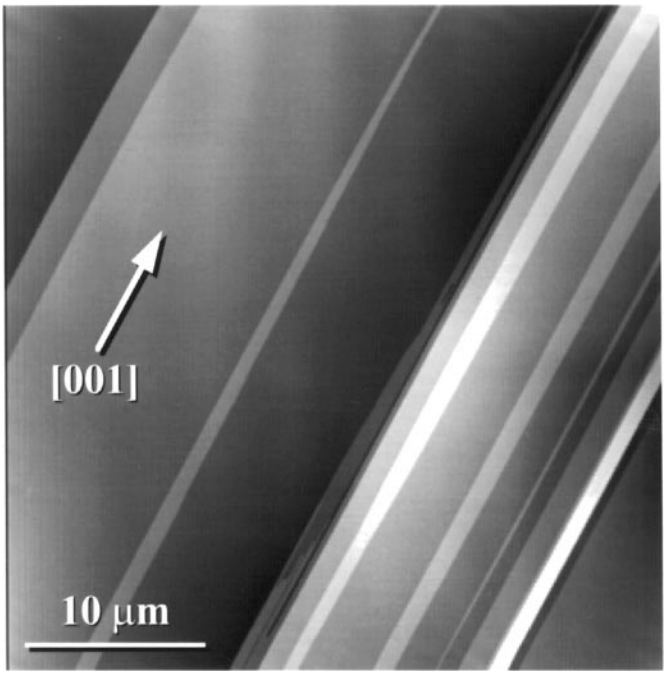

FIG. 1. A contact AFM image of the cleaved MoO_3(010) surface. Surface steps characteristically run parallel to [001]. The steps in this image all have heights that correspond to integer multiples of the 7 Å layer repeat unit in this structure; the highest is 21 Å.

RESULTS

(a) The MoO_3(010) Cleavage Surface

The freshly cleaved MoO_3(010) surface is characterized by large, atomically flat terraces separated by steps (see Fig. 1). The most common step-edge orientation is parallel to [001] and the heights of surface steps are always integer multiples of 7 Å. This distance is equal to one half of the oxide's **b** lattice vector and is also the distance between the van der Waals gaps that separate the adjacent double-octahedral layers of the structure. A more detailed description of the (010) surface structure has been presented earlier (24, 25).

(b) Reaction with $MeOH$–N_2

The atomically flat terraces of the MoO_3(010) surface are modified in two ways by a 2 min reaction in $MeOH$–N_2 at 400°C (see Fig. 2a). First, crystallographic shear (CS) planes intersect the surface parallel to the [001] direction. In AFM images, these defects appear as 1.5 Å high surface steps with edges parallel to [001] (24, 25). The observation of CS plane formation under these conditions is consistent with previous *in situ* TEM studies (21) and is indicative of oxygen deficient MoO_{3-x}. The second modification is the nucleation of small acicular precipitates along well defined directions of the MoO_3(010) surface plane. The angle between the axis of each precipitate and the [001] direction is $35.5^\circ \pm 2^\circ$ and we assign this to the ⟨203⟩ direction, which is inclined from the [001] axis by 35.56°. The precipitates are up to a few microns long (parallel to ⟨203⟩) and, as is evident by their white contrast in AFM images, they protrude from the (010) surface. After 2 min, the precipitates rise above the MoO_3 matrix by 5–10 Å.

The concentration, lateral size, and height of the ⟨203⟩ precipitates increase with the extent of the reaction. After 4 min, they are up to 10 μm in length and rise above the MoO_3 matrix by approximately 30 Å (see Fig. 2b). After 6 min (see Fig. 2c), the length and height of the precipitates can be up to 40 μm and 90 Å, respectively. During later stages of the reaction, new surface steps form parallel to [001]. These step defects, which can be seen in Fig. 2c, often originate near the end of a precipitate and we distinguish them from surface/CS plane intersections because their height is typically greater than 20 Å. After a 10 min reaction at 400°C in $MeOH$–N_2 (see Fig. 2d), the surface microstructure is dominated by large ⟨203⟩ precipitates that can have lengths in excess of 100 μm and heights of up to 200 Å. At this stage, the precipitates can easily be observed with a conventional optical microscope. Time-lapse studies, in

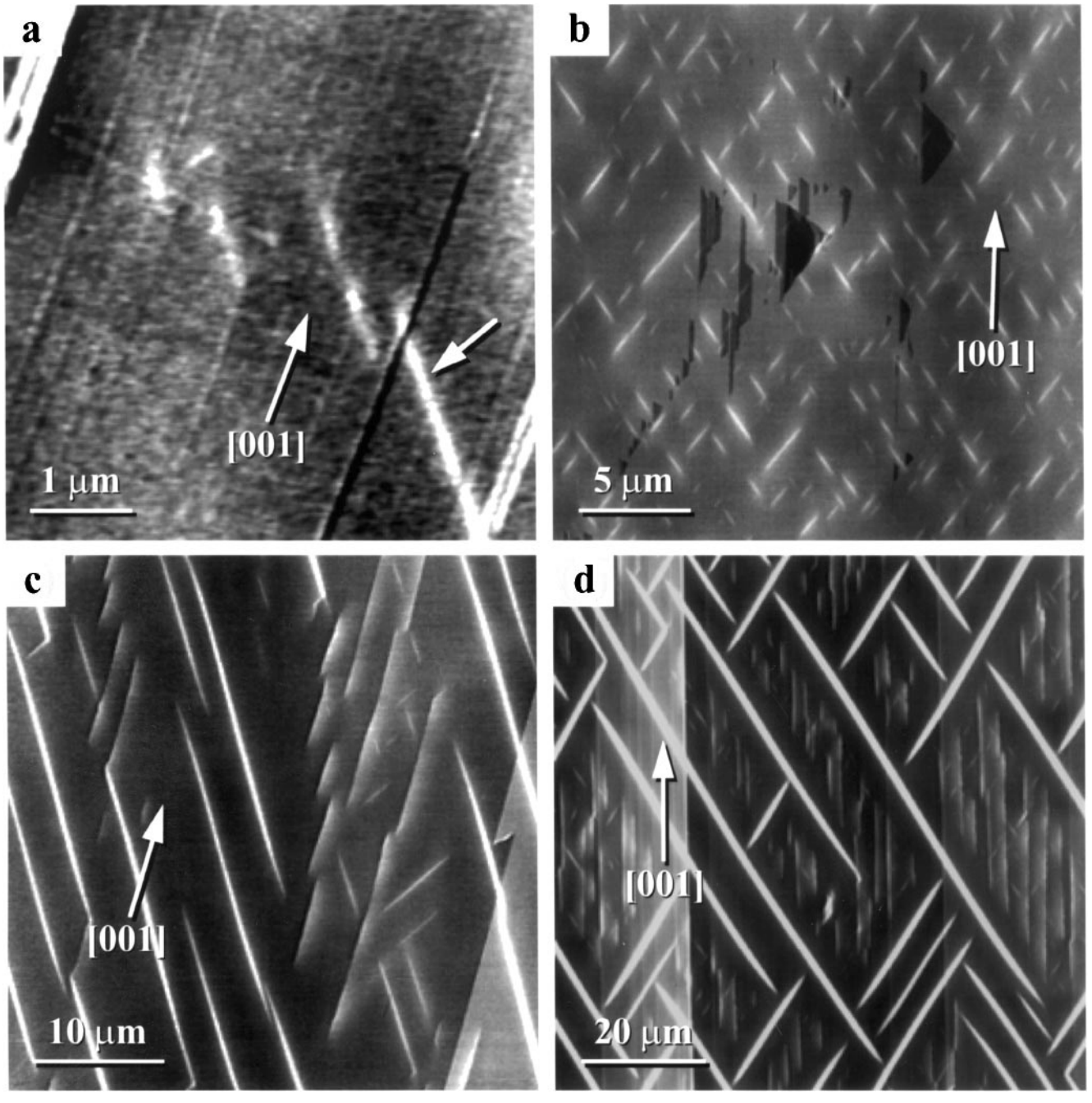

FIG. 2. (a) Contact AFM image of an MoO_3(010) surface reacted with a $MeOH–N_2$ mixture for 2 min at 400°C. Crystallographic shear (CS) planes are visible along [001] and small, needle-like precipitates (arrowed) have formed along the ⟨203⟩ axis of the (010) surface plane. The light-to-dark contrast in this image is 20 Å. (b) AFM image after a 4 min reaction in $MeOH–N_2$ at 400°C. The darkest features are lower terraces bounded by closed loop steps. These features were observed after the cleave and were unchanged by the reaction. The light-to-dark contrast in this image is 40 Å. (c) Extended reaction times (6 min) lead to enlarged precipitates and new step-defects along [001]. The light-to-dark contrast in this image is 150 Å. (d) MoO_3(010) surface microstructure after reacting for 10 min in $MeOH–N_2$ at 400°C. The light-to-dark contrast is 300 Å.

which the same areas of the surface were imaged after consecutive 2 min heating intervals, demonstrated that many of the precipitates which nucleated during the first treatment grew during subsequent treatments and that new precipitates continued to form. This suggests that the precipitates persist throughout the heating and cooling cycle. Finally, as the reaction progresses, the color of the single crystal surface changes from transparent, pale green (fresh) to transparent dark blue ($t \approx 4$ min) to opaque blue-purple ($t \approx 10$ min).

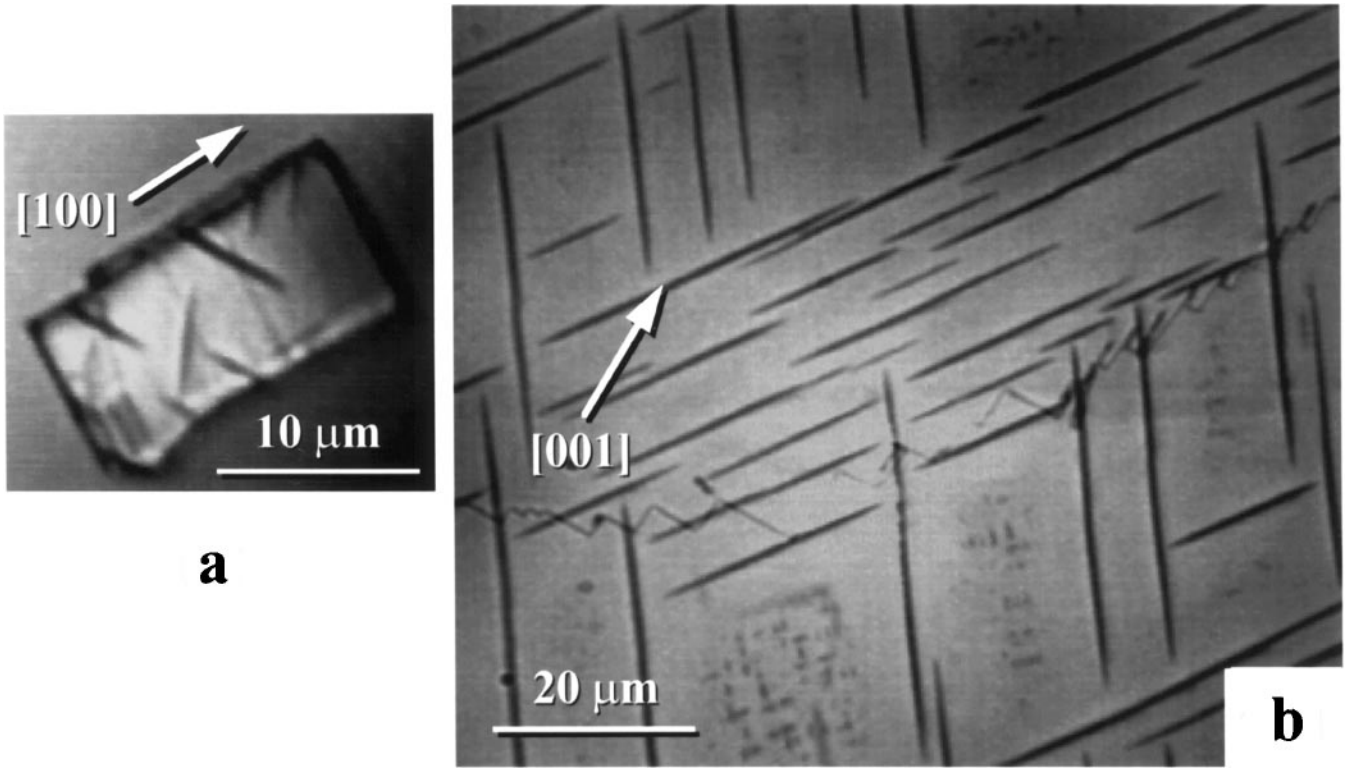

FIG. 3. (a) Optical micrograph of a small MoO_3 crystallite after a 15 min reaction with $MeOH–N_2$ at 300°C. (b) Optical micrograph of an MoO_3(010) surface which was reacted with $MeOH–N_2$ for 60 min at 300°C. At this stage, the precipitates are approximately 100 Å high. In optical micrographs, the ⟨203⟩ precipitates exhibit a dark contrast.

Identical ⟨203⟩ precipitates form on MoO_3(010) surfaces reacted with $MeOH–N_2$ mixtures at 300°C. At this temperature, however, CS plane/surface intersections and the large [001] step defects were not observed. At 300°C, the nucleation and growth rates of the precipitates are significantly slower than what is observed at 400°C. For example, after reaction times of 15 min, the observed precipitates are small and often confined to local regions of the crystal's surface. However, small crystallites (see Fig. 3a), which are reacted along with the single crystal, always contain the precipitates and they can be resolved with an optical microscope. After one hour at 300°C, the (010) surface is populated with large ⟨203⟩ precipitates with sizes and concentrations comparable to those observed after 10 min at 400°C (see Fig. 3b). Surfaces reacted in $MeOH–N_2$ at 200°C were unchanged after reaction times of up to two hours.

X-ray diffraction was used to unambiguously identify the ⟨203⟩ precipitates which form during the reaction with MeOH. First, several MoO_3 single crystals were reacted with $MeOH–N_2$ for 10 min at 400°C to produce a surface microstructure dominated by the large acicular precipitates, as in Fig. 2d. Subsequently, thin surface layers, rich in the precipitate phase, were cleaved from these crystals with adhesive tape, pulverized, and subjected to powder XRD analysis. The powder pattern from these reacted surface layers clearly shows that it is a two phase mixture. In Fig. 4, a

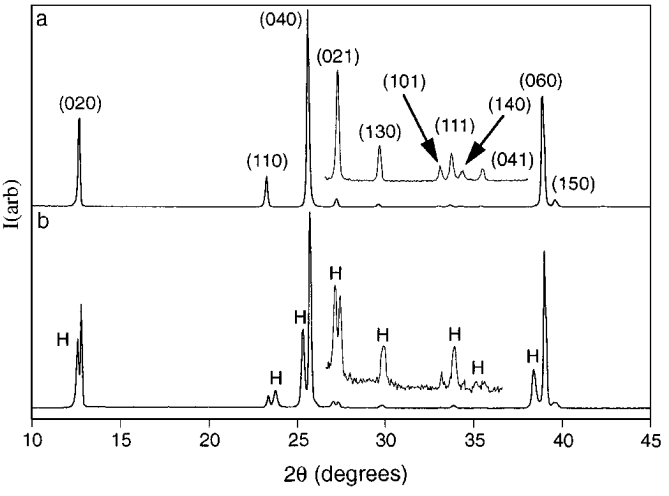

FIG. 4. (a) Powder XRD pattern of unreacted MoO_3. This phase has a primitive orthorhombic cell (Pbnm) and its lattice parameters are **a** = 3.963 Å, **b** = 13.856 Å, **c** = 3.6966 Å. The section between 26 and 37° is magnified in the inset to show detail. (b) Powder XRD pattern of pulverized surface layers, cleaved from MoO_3 single crystals reacted for 10 min in $MeOH/N_2$ at 400°C. Peaks that do not arise from MoO_3 are labeled with an H. This subset of new peaks can be fully indexed to the C-centered orthorhombic cell (Cmcm) of H_xMoO_3, where $0.23 \leq x \leq 0.4$ (25); its lattice parameters are **a** = 3.8830(8) Å, **b** = 14.0538(25) Å, **c** = 3.7282(16) Å. The (130) and (111) peaks of both phases overlap and the (101) and (140) peaks of the H-bronze are absent due to the Bravais lattice symmetry.

portion of the XRD pattern from the reacted surface layers is compared to that of unreacted MoO_3 so that the peaks from the second phase can be easily identified. The new peaks in the XRD pattern of the reacted material, which we associate with the ⟨203⟩ precipitates, can be indexed to a C-centered orthorhombic cell with refined lattice parameters (**a** = 3.8830 (9), **b** = 14.0538 (25), **c** = 3.7282 (16)) identical to those of the hydrogen bronze phase, H_xMoO_3, where $0.23 \leq x \leq 0.4$ (26). Every peak in the XRD pattern can be indexed to either MoO_3 or H_xMoO_3. A search of the JCPDS-ICDD file revealed that the hydrogen bronze, H_xMoO_3, is the only known phase containing combinations of Mo, O, C, N, or H that has a structure and lattice parameters consistent with the diffraction patterns.

The cleaved surface layers from samples treated for 1 h at 300°C in MeOH–N_2 give identical X-ray diffraction patterns. Because these samples do not contain CS planes or step defects, we can be confident in our association of the new diffraction peaks with the ⟨203⟩ precipitates. Powdered MoO_3 samples reacted with MeOH–N_2 at 300°C for 30 min had an improved signal-to-noise ratio and exhibited the same characteristic peaks of H_xMoO_3. These powder patterns confirmed the lattice parameters of the bronze and displayed the systematic absences characteristic of space group Cmcm. Finally, like the patterns from cleaved surface layers, all the peaks in the powder pattern could be indexed to either MoO_3 or H_xMoO_3.

Diffraction experiments with reacted single crystals demonstrated that the **b** lattice vectors of the matrix and the H_xMoO_3 precipitates are parallel. Thus, this transformation progresses in a topotactic manner that is characteristic of intercalation reactions (32). Because the b lattice parameter of the protonated phase is 0.2 Å larger than that of pure MoO_3, the precipitates swell 0.2 Å above the matrix phase for every unit layer of the structure that has been transformed to H_xMoO_3. This swelling gives rise to the white contrast that we associate with the precipitates in AFM images. Based on this geometric relationship between the precipitates and the matrix, a 200 Å high precipitate consists of 1000 unit layers of H_xMoO_3 and has a thickness of approximately 1.4 μm parallel to **b**.

(c) Reactions with EtOH and PrOH

Additional experiments were conducted to explore the conditions under which H_xMoO_3 forms during gas phase redox reactions. When analogous experiments were conducted with N_2–EtOH and N_2–PrOH mixtures, identical ⟨203⟩ oriented precipitates were observed with AFM and X-ray diffraction patterns from the reacted surface layers of these crystals showed the same characteristic peaks of H_xMoO_3. For example, the XRD patterns from surface layers reacted at 400°C for 15 and 12 min in EtOH and PrOH, respectively, were similar in appearance to XRD patterns from surfaces layers reacted in MeOH for 10 min (Fig. 4b). Topographic AFM images of MoO_3(010) surfaces reacted with EtOH and PrOH at 400°C are presented in Figs. 5a and b, respectively.

Protonation does not occur when MoO_3(010) cleavage surfaces are reacted with N_2, 10% H_2–N_2, or CO between

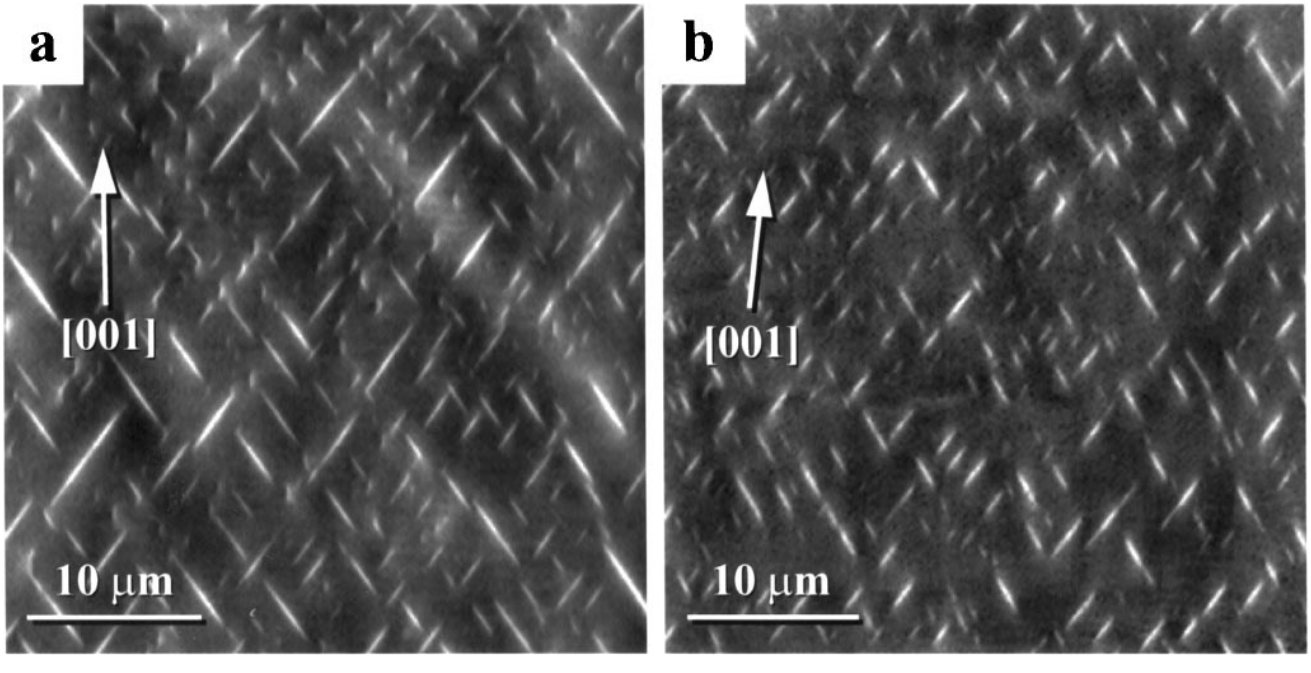

FIG. 5. Contact AFM images of MoO_3(010) surfaces reacted with (a) EtOH–N_2 and (b) 2-PrOH–N_2 mixtures at 400°C for 5 min. The white to black contrast in these images is approximately 50 Å.

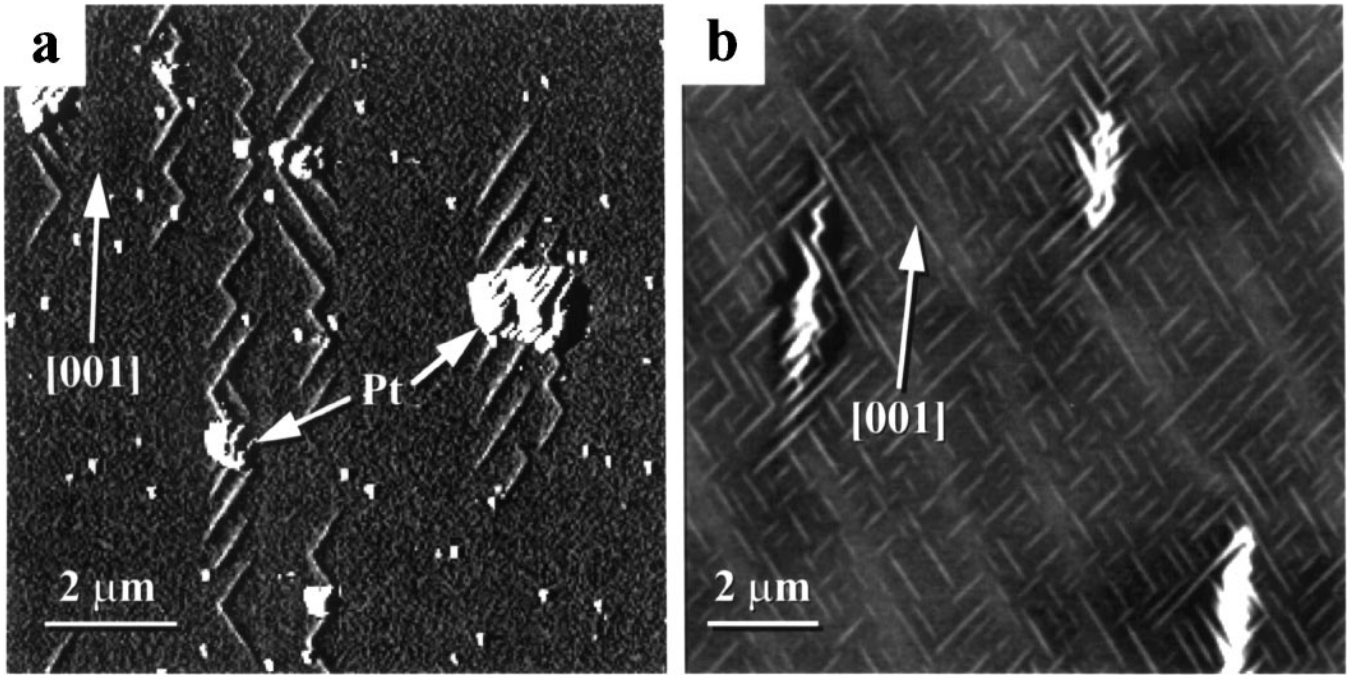

FIG. 6. (a) AFM deflection image of a Pt-supporting MoO_3(010) surface after reaction with 10% H_2–N_2 at 130°C for 60 min. For clarity, two of the Pt particles are arrowed in the figure. (b) AFM topograph of an MoO_3(010) surface which was covered with a ~1 mm thick layer of Pt black and reacted with 10% H_2–N_2 for 30 min at 130°C. The white-to-black contrast in this image is 50 Å.

200 and 400°C. Precipitates were not observed with AFM on surfaces reacted for as long as 15 min at 400°C and XRD patterns from the reacted surface layers of these crystals were characteristic of single phase MoO_3. Re-examination of reactions with 10% H_2–N_2 confirmed previous AFM observations (24); reaction with forming gas above 350°C leads to the formation of surfaces/CS plane intersections and surface voids. MoO_3(010) surfaces reacted with CO or N_2 with residual water (~20 ppm) above 350°C exhibit the same microstructural modifications as surfaces reacted with forming gas. If the CO or N_2 is dried prior to reaction, CS planes form, but surface voids do not. During low temperature ($T \leq 300$°C) reactions with dry forming gas, N_2, or CO, the MoO_3(010) surface structure is apparently unmodified. For example, after reactions in excess of 4 h at 300°C in 10% H_2–N_2, the reaction surface can not be distinguished from the fresh cleaved surface by AFM. Crystals treated for this long do, however, begin to turn blue, indicating that they are oxygen deficient (MoO_{3-x}). This observation demonstrates a limitation of the AFM when used at its nominal resolution; because only defects that create an extended deviation in the surface topography are easily imaged, we are unable to resolve the O vacancies which are certainly present at the surface.

(d) Reaction with Atomic H - Hydrogen Spill Over

H_xMoO_3 is a well-known product of reactions with atomic H produced by "spill over" from supported or admixed Pt particles (26–30). When Pt-supporting MoO_3 single crystals are reacted with dry forming gas (10% H_2–N_2) at 130°C, the (010) surface is modified in a manner similar to that observed during reactions with alcohols. The AFM deflection image in Fig. 6a shows a Pt-supporting (010) surface after reaction with forming gas for 60 min at 130°C. Small, acicular precipitates, oriented along ⟨203⟩, originate at the Pt particles and form preferentially along the [001] axis of the MoO_3 matrix. In topographic AFM images, the precipitates appear as a white contrast and, therefore, they rise, up to 30 Å, above the surface of the matrix.

When crystals are reacted with excess Pt, by covering the surface with a thick (~1 mm) layer of Pt black, the formation of the ⟨203⟩ precipitates is significantly faster. After 30 min at 130°C, most of the (010) surface is decorated with a well-developed, cross-hatched pattern of ⟨203⟩ precipitates, as in Fig. 6b. The regions of the surface which do not contain the ⟨203⟩ precipitates "roughen" to the extent that they are nearly impossible to image with AFM. The surface topography in these "rough" regions typically shows height variations in excess of 5 μm. These large (up to 40,000 μm^2) areas are always elongated along [001] and are distinguishable, in the optical microscope, by their dark blue color. The highest concentration of ⟨203⟩ precipitates is usually found directly adjacent to these rough areas of the (010) surface. We presume that these optically distinct regions reacted (protonated) at an accelerated pace. Finally, note that new [001] steps also form during this reaction (see

Fig. 6b). These small steps may be precursors to the macroscopic [001] steps which have been observed optically on MoO_3 crystals which had been transformed to $H_{1.68}MoO_3$ by spill over (29, 30).

Phase analysis, with XRD, of the surface layers of crystals reacted with a Pt excess for 30 min and Pt/MoO_3 powders reacted for as little as 2 min in 10% $H-N_2$ confirmed the expected presence of MoO_3 and H_xMoO_3. However, in addition to the hydrogen bronze with $0.23 \leq x \leq 0.4$, a second intercalated phase with $0.85 \leq x \leq 1.04$ (28), was also present. We assume that the less protonated phase is the first to form and, therefore, corresponds to the ⟨203⟩ precipitates which originate at the Pt particles (Fig. 6a) on Pt-supporting surfaces. The higher H content bronze is most likely present in the rough, optically distinct regions that were observed on the single crystal surfaces reacted with excess Pt.

When Pt-supporting or Pt excess samples were reacted with dry CO or N_2, H_xMoO_3 precipitates were not observed with AFM, even after reactions in excess of three hours at 130°C. With the exception of the presence of Pt particles, AFM images of these surfaces were indistinguishable from those of the fresh cleavage surface. XRD analysis of powdered Pt/MoO_3 samples which were reacted in dry CO for various times between 1 and 24 h at 130°C always proved to be a mixture of only MoO_3 and Pt.

DISCUSSION

Based on the evidence presented in the results section, we conclude that the ⟨203⟩-oriented precipitates which form on the MoO_3(010) surface during reactions with alcohols are the hydrogen molybdenum bronze phase, H_xMoO_3, where $0.23 \leq x \leq 0.4$ (28). The support for this assignment is based not only on observations during reactions with alcohols, but also on observations during H spill over reactions, where the relevant intercalation chemistry is already well established by earlier studies (26–30). During H spill over, atomic H dissolves into MoO_3 after H_2 is dissociated by the Pt catalyst. Furthermore, when the MoO_3(010) surface was treated in environments from which atomic H was excluded (for example, N_2 or CO), the ⟨203⟩-oriented precipitates never formed. Our results show that during reactions with alcohols, H removed from the alcohol during the oxidation reaction dissolves into MoO_3.

Our observation that H_xMoO_3 forms as a by-product of reactions with alcohols is consistent with earlier XRD studies (7, 8). The habit and morphology of the observed H_xMoO_3 precipitates are identical to microstructural features called domains that have been observed during past TEM experiments (9–21, 23). The domains were first reported more than 50 years ago and have been described in different ways and with different indices. While some groups have also described the orientation as the ⟨203⟩ direction (15), which makes a 35.54° angle with [001], Gai and co-workers (20, 21, 23) indexed the direction as ⟨304⟩, which makes a 38.8° angle with [001]. However, regardless of this choice, a comparison of the micrographs in the references cited above makes it clear that the various groups observed the same two-phase microstructure. The domains have been observed both during beam heating in the microscope's vacuum (9–15) and during *in situ* reduction in an environmental cell (16–18, 20, 21, 23). Selected area electron diffraction patterns indicate that the structure of the domains is similar to that of the MoO_3 matrix (14, 15, 20, 23) and this observation has been interpreted in two different ways.

The first interpretation, provided by Bursill *et al.* (15), is that the domains are a hydrogen molybdenum bronze, H_xMoO_3, formed due to the incorporation of surface hydroxyl impurities during beam heating. In this case, the phase identification was supported by convergent beam electron diffraction results which demonstrated that the domains exhibited the same space group and **a** and **c** lattice parameters as the hydrogen bronze $Mo_4O_{10}(OH)_2$ (31). This oxy-hydroxide phase has more recently been formulated as H_xMoO_3, where $0.23 \leq x \leq 0.4$, and we prefer that latter of the two expressions (28). Since the samples used in the current study were at the opposite extreme with respect to the surface-to-volume ratio, we do not expect the incorporation of surface hydroxyls to saturate the bulk and lead to precipitation of the bronze. This is consistent with our observation that the ⟨203⟩-precipitates only form in conditions where H was available either from the spill-over reaction or from the decomposition of alcohol. In all other respects, our conclusions regarding the nature of the precipitates are consistent with those of Bursill *et al.* (15). It should be noted that the tendency of MoO_3 to react with trace H impurities is well documented and supports this model. For example, in ultrahigh vacuum, with gaseous H_2 at pressures as low as 10^{-8} torr, hydrogen molybdenum bronzes are formed when MoO_3 is placed in the vicinity of a hot W filament (30). Without the filament, the reaction can still be catalyzed at this low pressure either by Pt or by the bronze itself (29, 30). In fact, there are a wide variety of conditions under which this phase is known to form (26–32).

The second interpretation, provided by Gai *et al.* (20, 21, 23), is that the domains are an oxygen deficient phase having an ordered arrangement of oxygen vacancies. This assignment was supported on the basis of selected area electron diffraction patterns. However, it had already been demonstrated by Bursill *et al.* (15) that these same patterns were entirely consistent with the presence of the H-bronze phase. While the H-bronze phase was already well characterized at the time, the superlattice phase proposed by Gai *et al.* (20, 21, 23) has never been detected in any other study of the Mo–O system (33, 34). Furthermore, the current and previous XRD studies (7, 8) show no evidence for the

superlattice peaks expected from the proposed O-deficient phase. Gai *et al*. (21) provided two reasons for rejecting the idea that the domains were a H-bronze. The first is that the domains form in all environments, even CO/He mixtures where no source of H is thought to be present. However, this is not inconsistent with the model proposed by Bursill *et al*. (15). If the H-bronze phase is actually formed from surface hydroxyl impurities, then the source of H is from the sample itself and the environment is irrelevant. In fact, none of the TEM studies cite any conditions under which the domains do not form. This observation supports the idea that the formation mechanism is related to the high surface area sample itself and/or the inevitable electron irradiation that occurs during TEM observations. The second reason for rejecting the earlier assignment was the erroneous assumption that the H-bronze is not stable above 200°C (21). In fact, the existing data indicate that the hydrogen molybdenum bronze is stable until at least 390°C during vacuum heating (35). We expect this stability range to be extended when the activity of H in the ambient is increased, as it is during the dissociative chemisorption of an alcohol. In summary, the observations described by Gai *et al*. (20, 21, 23) provide no evidence to contradict the conclusion that the ⟨203⟩-oriented precipitates are H_xMoO_3.

In the present study, the well defined conditions under which the precipitates are observed combined with the XRD signature of H_xMoO_3 leave little doubt that the ⟨203⟩-oriented precipitates which form during H spill over and reactions with alcohols are H_xMoO_3. Considering the wide variety of conditions under which this phase is known to form (26–32), its precipitation during reactions with alcohols is not too surprising. In fact, earlier XRD studies showed that the H-bronze formed after low temperature annealing in methanol (7, 8) and the authors of an earlier report on the oxidation of methanol by MoO_3 speculated on the possibility of hydrogen bronze formation as the surface methoxy decomposes to yield formaldehyde (4). Based on the new evidence presented here, it is interesting to reconsider the mechanism of alcohol oxidation on MoO_3.

When an alcohol molecule is oxidized by MoO_3, two hydrogens are removed. According to the accepted model, the first is removed during the initial dissociative chemisorption of the alcohol and the second is removed when the surface alkoxy decomposes to the aldehyde. Both liberated protons are thought to react with lattice O to form H_2O and a surface oxygen vacancy (2, 3). Under the experimental conditions detailed here, however, some portion of the liberated H intercalates into the MoO_3 lattice and H_xMoO_3 is formed. The H that reacts with MoO_3 might be formed during the dissociative chemisorption, the alkoxide decomposition, or both steps. Farneth *et al*. (4) suggested that bronze formation might explain the temperature lag between aldehyde desorption and H_2O desorption during TPD of MeOH and EtOH from MoO_3. However, this temperature lag is not observed during TPD of 2-PrOH and we still observe H_xMoO_3 precipitation during this reaction (3). Machiels and Sleight (1) have studied MeOH oxidation in the absence of gas phase O_2 (conditions identical to those studied here). Because the product distribution they observed included dimethyl ether, H_2, and methane, but not formaldehyde, we surmise that while the dissociative chemisorption of MeOH still occurs, the decomposition of the methoxy to formaldehyde does not occur. This suggests that in our case, the bronze must be formed during the dissociative chemisorption of the alcohol (although we cannot rule out the possibility of protonation during both steps of the reaction). The formation of this protonated phase implies that H can be removed from the alcohol without creation of an O vacancy, a process that might become more important at lower temperatures where vacancy generation is less probable.

There are a number of materials properties often associated with partial oxidation catalysts. For example, they must be able to easily form and transport stoichiometry compensating defects. Considering the fact that many of the molybdates and vanadates used as oxidation catalysts are able to form H-bronzes or at least dissolve some H (36), it is interesting to speculate that this also is an important, but previously unrecognized, property of useful partial oxidation catalysts.

ACKNOWLEDGMENTS

This work was supported by the National Science Foundation under YIA Grant DMR-9458005. The authors also thank G. W. Coulston and W. E. Farneth for their useful comments.

REFERENCES

1. Machiels, C. J., and Sleight, A. W., *in* "Proceedings of the 4th International Conference on the Chemistry and Uses of Molybdenum" (H. F. Barry and P. C. H. Mitchell, Eds.), p. 411. Climax Molybdenum Co., Ann Arbor, MI, 1982.
2. Farneth, W. E., Ohuchi, F., Staley, R. H., Chowdhry, U., and Sleight, A. W., *J. Phys. Chem*. **89**, 2493 (1985).
3. Farneth, W. E., Staley, R. H., and Sleight, A. W., *J. Am. Chem. Soc.* **108**, 2327 (1986).
4. Farneth, W. E., McCarron, III, E. M., Sleight, A. W., and Staley, R. H., *Langmuir* **3**, 217 (1987).
5. Mars, R., and van Krevelen, D. W., *Chem. Eng. Sci.* **3**, 41 (1954).
6. Haber, J., *in* "Solid State Chemistry in Catalysis" (R. Grasselli and J. Brazdil, Eds.), p. 1. American Chemical Society, Washington, DC, 1985.
7. Vergnon, P., and Tatibouet, J. M., *Bull. Soc. Chim. Fr.* **11–12**, 455 (1980).
8. Guidot, J., and Germain, J. E., *React. Kinet. Catal. Lett.* **15**, 389 (1980).
9. Heidenreich, R. D., and Sturkey, L., *J. Appl. Phys.* **16**, 97 (1945).
10. Glemser, O., and Lutz, G., *Kolloid-Z*. **119**, 99 (1950).
11. König, H., *Z. Physik*. **130**, 483 (1951).
12. Hashimoto, H., *J. Phys. Soc. Japan* **9**, 150 (1954).
13. Pernoux, E., and Borrelly, R., *J. Microscopie* **2**, 407 (1963).
14. Bursill, L. A., *Proc. Roy. Soc.* **A311**, 267 (1969).

15. Bursill, L. A., Dowell, W. C. T., Goodman, P., and Tate, N., *Acta Cryst.* **A34**, 296 (1974).
16. Thöni, W., and Hirsch, P. B., *Phil. Mag.* **33**, 639 (1976).
17. Thöni, W., Gai, P. L., and Hirsch, P. B., *Phil. Mag.* **35**, 781 (1977).
18. Thöni, W., Gai, P., and Hirsch, P. B., *J. Less-Common Metals* **54**, 263 (1977).
19. Bertrand, O., and Dufour, L. C., *Phys. Stat. Sol. A* **60**, 507 (1980).
20. Gai, P. L., *Phil. Mag. A* **43**, 841 (1981).
21. Gai, P. L., and Labun, P. A., *J. Catal.* **94**, 79 (1985).
22. Hansen, S., and Andersson, A., *J. Solid State Chem.* **75**, 225 (1988).
23. Gai-Boyes, P. L., *Catal. Rev.-Sci. Eng.* **34**, 1 (1992).
24. Smith, R. L., and Rohrer, G. S., *J. Catal.* **163**, 12 (1996).
25. Smith, R. L., and Rohrer, G. S., *J. Solid State Chem.* **124**, 104 (1996).
26. Sermon, P. A., and Bond, G. C., *Catal. Rev.* **8**, 211 (1973).
27. Sermon, P. A., and Bond, G. C., *J. Chem. Soc. Faraday I* **72**, 730 (1976).
28. Birtill, J. J., and Dickens, P. G., *Mat. Res. Bul.* **13**, 311 (1978).
29. Erre, R., van Damme, H., and Fripiat, J. J., *Surf. Science* **127**, 48 (1983).
30. Erre, R., Legay, M. H., and Fripiat, J. J., *Surf. Science* **127**, 69 (1983).
31. Glemser, O., and Lutz, G., *Z. Anorg. Allg. Chem.* **264**, 17 (1951).
32. Jacobson, A. J., *in* "Solid State Chemistry Compounds" (A. K. Cheetham and P. Day, Eds.), p. 182. Clarendon Press, Oxford. 1992.
33. Kihlborg, L., *Ark. Kemi* **21**, 471 (1963).
34. Chang, L. L. Y., and Phillips, B., *J. Am. Ceram. Soc.* **52**, 527 (1969).
35. Sotani, N., Kowamoto, Y., and Inui, M., *Mat. Res. Bull.* **18**, 797 (1983).
36. Schöllhorn, R., *Angew. Chem. Int. Ed. Engl.* **19**, 983 (1980).